

Big bang nucleosynthesis limit on N_ν

E. Lisi ^{a*}, S. Sarkar ^{b†} and F.L. Villante ^{c‡}

^a*Dipartimento di Fisica and Sezione INFN di Bari, Via Amendola 173, I-70126 Bari, Italy*

^b*Theoretical Physics, University of Oxford, 1 Keble Road, Oxford OX1 3NP, UK*

^c*Dipartimento di Fisica and Sezione INFN di Ferrara, Via del Paradiso 12, I-44100 Ferrara, Italy*

(March 25, 2018)

Abstract

Recently we presented a simple method for determining the correlated uncertainties of the light element abundances expected from big bang nucleosynthesis, which avoids the need for lengthy Monte Carlo simulations. We now extend this approach to consider departures from the Standard Model, in particular to constrain any new light degrees of freedom present in the thermal plasma during nucleosynthesis. Since the observational situation regarding the inferred primordial abundances has not yet stabilized, we present illustrative bounds on the equivalent number of neutrino species N_ν for various combinations of individual abundance determinations. Our 95% C.L. bounds on N_ν range between 2 and 4, and can easily be reevaluated using the technique provided when the abundances are known more accurately.

26.35.+c, 98.80.Ft, 14.60.St

Typeset using REVTeX

*Eligio.Lisi@ba.infn.it

†S.Sarkar@physics.ox.ac.uk

‡Villante@fe.infn.it

I. INTRODUCTION

The Standard Model (SM) contains only $N_\nu = 3$ weakly interacting massless neutrinos. However the recent experimental evidence for neutrino oscillations [1] may require it to be extended to include new superweakly interacting massless (or very light) particles such as singlet neutrinos or Majorons. These do not couple to the Z^0 vector boson and are therefore not constrained by the precision studies of Z^0 decays which establish the number of $SU(2)_L$ doublet neutrino species to be [2]

$$N_\nu = 2.993 \pm 0.011. \quad (1)$$

However, as was emphasized some time ago [3], such particles would boost the relativistic energy density, hence the expansion rate, during big bang nucleosynthesis (BBN), thus increasing the yield of ^4He . This argument was quantified for new types of neutrinos and new superweakly interacting particles [4] in terms of a bound on the *equivalent number of massless neutrinos* present during nucleosynthesis:

$$N_\nu = 3 + f_{\text{B,F}} \sum_i \frac{g_i}{2} \left(\frac{T_i}{T_\nu} \right)^4, \quad (2)$$

where g_i is the number of (interacting) helicity states, $f_{\text{B}} = 8/7$ (bosons) and $f_{\text{F}} = 1$ (fermions), and the ratio T_i/T_ν depends on the thermal history of the particle under consideration [5]. For example, $T_i/T_\nu \leq 0.465$ for a particle which decouples above the electroweak scale such as a singlet Majoron or a sterile neutrino. However the situation may be more complicated, e.g. if the sterile neutrino has large mixing with a left-handed doublet species, it can be brought into equilibrium through (matter-enhanced) oscillations in the early universe, making $T_i/T_\nu \simeq 1$ [6]. Moreover such oscillations can generate an asymmetry between ν_e and $\bar{\nu}_e$, thus directly affecting neutron-proton interconversions and the resultant yield of ^4He [7]. This can be quantified in terms of the *effective* value of N_ν parametrizing the expansion rate during BBN, which may well be below 3! Similarly, non-trivial changes in N_ν can be induced by the decays [8] or annihilations [9] of massive neutrinos (into e.g. Majorons), so it is clear that it is a sensitive probe of new physics.

The precise bound on N_ν from nucleosynthesis depends on the adopted primordial elemental abundances as well as uncertainties in the predicted values. Although the theoretical calculation of the primordial ^4He abundance is now believed to be accurate to within $\pm 0.4\%$ [10], its observationally inferred value as reported by different groups [11,12] differs by as much as $\approx 4\%$. Furthermore, a bound on N_ν can only be derived if the nucleon-to-photon ratio $\eta \equiv n_{\text{N}}/n_\gamma$ (or its lower bound) is known, since the effect of a faster expansion rate can be compensated for by the effect of a smaller nucleon density. This involves comparison of the expected and observed abundances of other elements such as D, ^3He and ^7Li which are much more poorly determined, both observationally and theoretically. The most crucial element in this context is deuterium which is supposedly always destroyed and never created by astrophysical processes following the big bang [13]. Until relatively recently [14,15], its primordial abundance could not be directly measured and only an indirect upper limit could be derived based on models of galactic chemical evolution. As reviewed in ref. [16], the implied lower bound to η was then used to set increasingly stringent upper bounds on N_ν

ranging from 4 downwards [17], culminating in one below 3 which precipitated the so-called “crisis” for standard BBN [18], and was interpreted as requiring new physics.

However as cautioned before [19], there are large systematic uncertainties in such constraints on N_ν which are sensitive to our limited understanding of galactic chemical evolution. Moreover it was emphasized [20] that the procedure used earlier [17] to bound N_ν was statistically inconsistent since, e.g., correlations between the different elemental abundances were not taken into account. A Monte Carlo (MC) method was developed for estimation of the correlated uncertainties in the abundances of the synthesized elements [21,22], and incorporated into the standard BBN computer code [23], thus permitting reliable determination of the bound on N_ν from estimates of the primordial elemental abundances. Using this method, it was shown [24] that the *conservative* observational limits on the primordial abundances of D, ^4He and ^7Li allowed $N_\nu \leq 4.53$ (95% C.L.), significantly less restrictive than earlier estimates. Similar conclusions followed from studies using maximum likelihood (ML) methods [25–27]. However the use of the Monte Carlo method is computationally expensive and moreover the calculations need to be repeated whenever any of the input parameters — either reaction rates or inferred primordial abundances — are updated.

In a previous paper [28] we presented a simple method for estimation of the BBN abundance uncertainties and their correlations, based on linear error propagation. To illustrate its advantages over the MC+ML method, we used simple χ^2 statistics to obtain the best-fit value of the nucleon-to-photon ratio in the standard BBN model with $N_\nu = 3$ and indicated the relative importance of different nuclear reactions in determining the synthesized abundances. In this work we extend this approach to consider departures from $N_\nu = 3$. We have checked that our results are consistent with those obtained independently [29] using the MC+ML method [29,30] where comparison is possible.

The essential advantage of our method is that the correlated constraints on N_ν and η can be easily reevaluated using just a pocket calculator and the numerical tables provided, when the input nuclear reaction cross-sections or inferred abundances are known better. We have in fact embedded the calculations in a compact Fortran code, which is available upon request from the authors, or from a website [31]. Thus observers will be able to readily assess the impact of new elemental abundance determinations on an important probe of physics beyond the standard model.

II. THE METHOD

In this section we recapitulate the basics of our method [28] and outline its extension to the case $N_\nu \neq 3$.

A. Basic Ingredients

The method has both experimental and theoretical ingredients. The experimental ingredients are: (a) the inferred values of the primordial abundances, $\bar{Y}_i \pm \bar{\sigma}_i$; and (b) the nuclear reaction rates, $R_k \pm \Delta R_k$. We normalize [28] all the rates to a “default” set of values ($R_k \equiv 1$), namely, to the values compiled in Ref. [22], except for the neutron decay rate, which is updated to its current value [2].

The theoretical ingredients are: (a) the calculated abundances Y_i ; and (b) the logarithmic derivatives $\lambda_{ik} = \partial \ln Y_i / \partial \ln R_k$. Such functions have to be calculated for generic values of N_ν and of $x \equiv \log_{10}(\eta_{10})$, where $\eta_{10} = \eta/10^{-10}$. Note that the fraction of the critical density in nucleons is given by $\Omega_N h^2 \simeq \eta_{10}/273$, where $h \sim 0.7 \pm 0.1$ is the present Hubble parameter in units of $100 \text{ km s}^{-1} \text{ Mpc}^{-1}$, and the present temperature of the relic radiation background is $T_0 = 2.728 \pm 0.002 \text{ K}$ [2].

The logarithmic derivatives λ_{ik} can be used to propagate possible changes or updates of the input reaction rates ($R_k \rightarrow R_k + \delta R_k$) to the theoretical abundances ($Y_i \rightarrow Y_i + Y_i \lambda_{ik} \delta R_k / R_k$). Moreover, they enter in the calculation of the theoretical error matrix for the abundances, $\sigma_{ij}^2 = Y_i Y_j \sum_k \lambda_{ik} \lambda_{jk} (\Delta R_k / R_k)^2$. This matrix, summed to the experimental error matrix $\bar{\sigma}_{ij}^2 = \delta_{ij} \bar{\sigma}_i \bar{\sigma}_j$ and then inverted [28], defines the covariance matrix of a simple χ^2 statistical estimator. Contours of equal χ^2 can then be used to set bounds on the parameters (x, N_ν) at selected confidence levels.

In Ref. [28] we gave polynomial fits for the functions $Y_i(x, N_\nu)$ and $\lambda_{ik}(x, N_\nu)$ for $x \in [0, 1]$ and $N_\nu = 3$. The extension of our method to the case $N_\nu \neq 3$ (say, $1 \leq N_\nu \leq 5$) is, in principle, straightforward, since it simply requires recalculation of the functions Y_i and λ_{ik} at the chosen value of N_ν . However, it would not be practical to present, or to use, extensive tables of polynomial coefficients for many different values of N_ν . Therefore, we have devised some formulae which, to good accuracy, relate the calculations for arbitrary values of N_ν to the standard case $N_\nu = 3$, thus reducing the numerical task dramatically. Such approximations are discussed in the next subsection.

B. Useful Approximations

As is known from previous work [32], the synthesized elemental abundances D/H, $^3\text{He}/\text{H}$, and $^7\text{Li}/\text{H}$ (i.e., Y_2 , Y_3 , and Y_7 in our notation) are given to a good approximation by the quasi-fixed points of the corresponding rate equations, which formally read

$$\frac{dY_i}{dt} \propto \eta \sum_{+,-} Y \times Y \times \langle \sigma v \rangle_T, \quad (3)$$

where the sum runs over the relevant source (+) and sink (−) terms, and $\langle \sigma v \rangle_T$ is the thermally-averaged reaction cross section. Since the temperature of the universe evolves as $dT/dt \propto -T^3 \sqrt{g_\star}$, with the number of relativistic degrees of freedom, $g_\star = 2 + (7/4)(4/11)^{4/3} N_\nu$ (following e^+e^- annihilation), the above equation can be rewritten as

$$\frac{dY_i}{dT} \propto -\frac{\eta}{g_\star^{1/2}} T^{-3} \sum_{+,-} Y \times Y \times \langle \sigma v \rangle_T, \quad (4)$$

which shows that Y_2 , Y_3 , and Y_7 depend on η and N_ν essentially through the combination $\eta/g_\star^{1/2}$. Thus the calculated abundances Y_2 , Y_3 , and Y_7 (as well as their logarithmic derivatives λ_{ik}) should be approximately constant for

$$\log \eta - \frac{1}{2} \log g_\star = \text{const}, \quad (5)$$

as we have verified numerically.

Equation (5), linearized, suggests that the values of Y_i and of λ_{ik} for $N_\nu = 3 + \Delta N_\nu$ can be related to the case $N_\nu = 3$ through an appropriate shift in x :

$$Y_i(x, 3 + \Delta N_\nu) \simeq Y_i(x + c_i \Delta N_\nu, 3) , \quad (6)$$

$$\lambda_{ik}(x, 3 + \Delta N_\nu) \simeq \lambda_{ik}(x + c_i \Delta N_\nu, 3) , \quad (7)$$

where the coefficient c_i is estimated to be ~ -0.03 from Eq. (5) (at least for small ΔN_ν). In order to obtain a satisfactory accuracy in the whole range $(x, N_\nu) \in [0, 1] \times [1, 5]$, we allow upto a second-order variation in ΔN_ν , and for a rescaling factor of the Y_i 's:

$$Y_i(x, 3 + \Delta N_\nu) = (1 + a_i \Delta N_\nu + b_i \Delta N_\nu^2) Y_i(x + c_i \Delta N_\nu + d_i \Delta N_\nu^2, 3) , \quad (8)$$

$$\lambda_{ik}(x, 3 + \Delta N_\nu) = \lambda_{ik}(x + c_i \Delta N_\nu + d_i \Delta N_\nu^2, 3) . \quad (9)$$

We have checked that the above formulae (with coefficients determined through a numerical best-fit) link the cases $N_\nu \neq 3$ to the standard case $N_\nu = 3$ with very good accuracy.

As regards the ^4He abundance (Y_4 in our notation), a semi-analytical approximation also suggests a relation between x and N_ν similar to Eq. (5), although with different coefficients [33]. Indeed, functional relations of the kind (8,9) work well also in this case. However, in order to achieve higher accuracy and, in particular, to match the result of the recent precision calculation of Y_4 which includes all finite temperature and finite density corrections [10], we also allow for a rescaling factor for the λ_{4k} 's.

We wish to emphasize that the validity of our prescription [28] for the evaluation of the BBN uncertainties and for the χ^2 statistical analysis does *not* depend on the approximations discussed above. The semi-empirical relations (8,9) are only used to enable us to provide the interested reader with a simple and compact numerical code [31]. This allows easy extraction of joint fits to x and N_ν for a given set of elemental abundances, without having to run the full BBN code, and with no significant loss in accuracy.

III. PRIMORDIAL LIGHT ELEMENT ABUNDANCES

The abundances of the light elements synthesized in the big bang have been subsequently modified through chemical evolution of the astrophysical environments where they are measured [34]. The observational strategy then is to identify sites which have undergone as little chemical processing as possible and rely on empirical methods to infer the primordial abundance. For example, measurements of deuterium (D) can now be made in quasar absorption line systems (QAS) at high red shift; if there is a ‘‘ceiling’’ to the abundance in different QAS then it can be assumed to be the primordial value. The helium (^4He) abundance is measured in H II regions in blue compact galaxies (BCGs) which have undergone very little star formation; its primordial value is inferred either by using the associated nitrogen or oxygen abundance to track the stellar production of helium, or by simply observing the most metal-poor objects [35]. (We do not consider ^3He which can undergo both creation and destruction in stars [34] and is thus unreliable for use as a cosmological probe.) Closer to home, the observed uniform abundance of lithium (^7Li) in the hottest and most metal-poor Pop II stars in our Galaxy is believed to reflect its primordial value [36].

However as observational methods have become more sophisticated, the situation has become more, instead of less, uncertain. Large discrepancies, of a systematic nature, have

emerged between different observers who report, e.g., relatively ‘high’ [14,37,38] or ‘low’ [15,39,40] values of deuterium in different QAS, and ‘low’ [11,41] or ‘high’ [12,42] values of helium in BCG, using different data reduction methods. It has been argued that the Pop II lithium abundance [43–45] may in fact have been significantly depleted down from its primordial value [46,47], with observers arguing to the contrary [48]. We do not wish to take sides in this matter and instead consider several combinations of observational determinations, which cover a wide range of possibilities, in order to demonstrate our method and obtain illustrative best-fits for η and N_ν . The reader is invited to use the programme we have provided [31] to analyse other possible combinations of observational data.

A. Data Sets

The data sets we consider are tabulated in Table I. Below we comment in detail on our choices.

- Data Set A: This is taken from Ref. [29] who performed the first detailed MC+ML analysis to determine η and N_ν and is chosen essentially for comparison with our method, as in our previous paper [28].

Their adopted value of the primordial deuterium abundance, $\overline{Y}_2 = 1.9 \pm 0.4 \times 10^{-4}$, was based on early observations of a QAS at redshift $z = 3.32$ towards Q0014+813 which suggested a relatively ‘high’ value [14], and was consistent with limits set in other QAS, but in conflict with the much lower abundance found in a QAS at $z = 3.572$ towards Q1937-1009 [15]. More recently, observations of a QAS at $z = 0.701$ towards Q1718+4807 have also yielded a high abundance [37,38] as we discuss later.

The primordial helium abundance was taken to be $\overline{Y}_4 = 0.234 \pm 0.002 \pm 0.005$ from linear regression to zero metallicity in a set of 62 BCGs [41], based largely on observations which gave a relatively ‘low’ value [11].

Finally the primordial lithium abundance $\overline{Y}_7 = 1.6 \pm 0.36 \times 10^{-10}$ was taken from the Pop II observations of Ref. [44], assuming no depletion.

- Data Set B: This corresponds to the alternative combination of ‘low’ deuterium and ‘high’ helium, as considered in our previous work [28], with some small changes.

The primordial deuterium abundance, $\overline{Y}_2 = 3.4 \pm 0.3 \times 10^{-5}$, adopted here is the average of the ‘low’ values found in two well-observed QAS, at $z = 3.572$ towards Q1937-1009 [39], and at $z = 2.504$ towards Q1009+2956 [40].

The primordial helium abundance, $\overline{Y}_4 = 0.245 \pm 0.004$, is taken to be the average of the values found in the two most metal-poor BCGs, I Zw 18 and SBS 0335-052, from a new analysis which uses the helium lines themselves to self-consistently determine the physical conditions in the H II region, and specifically excludes those regions which are believed to be affected by underlying stellar absorption [42]. For example these authors demonstrate that there is strong underlying stellar absorption in the NW component of I Zw 18, which has been included in earlier analyses [11].

The primordial lithium abundance $\overline{Y}_7 = 1.73 \pm 0.21 \times 10^{-10}$ is from Ref. [45], again assuming no depletion. (Note that the uncertainty was incorrectly reported as $\pm 0.12 \times 10^{-10}$ in Ref. [36], as used in our previous work [28].)

- **Data Set C:** It has been suggested [49] that the discordance between the ‘high’ and ‘low’ values of the deuterium abundance reported in QAS may be considerably reduced if the analysis of the H+D profiles accounts for the correlated velocity field of bulk motion, i.e. mesoturbulence, rather than being based on multi-component microturbulent models. It is then found [49] that a value of $\overline{Y}_2 = (3.5 - 5.2) \times 10^{-5}$ is compatible simultaneously (at 95% C.L.) with observations of the QAS at $z = 0.701$ towards Q1718+4807 (in which a ‘high’ value was reported [37,38]), and observations of the QAS at $z = 3.572$ towards Q1937-1009 and at $z = 2.504$ towards Q1009+2956 (in which a ‘low’ value was reported [39,40]). We adopt this value, along with the same helium abundance as in Set B.

It has also been argued that the lithium abundance observed in Pop II stars has been depleted down from a primordial value of $\overline{Y}_7 = 3.9 \pm 0.85 \times 10^{-10}$ [50], the lower end of the range being set by the presence of highly overdepleted halo stars and consistency with the ${}^7\text{Li}$ abundance in the Sun and in open clusters, while the upper end of the range is set by the observed dispersion of the Pop II abundance “plateau” and the ${}^6\text{Li}/{}^7\text{Li}$ depletion ratio. We adopt this value, noting that a somewhat smaller depletion is suggested by other workers [47] who find a primordial abundance of $\overline{Y}_7 = 2.3 \pm 0.5 \times 10^{-10}$.

- **Data Set D:** Recently, a ‘high’ value of the deuterium abundance, $\overline{Y}_2 = 3.3 \pm 1.2 \times 10^{-4}$, has been reported from observations of a QAS at $z = 0.701$ towards Q1718+4807 [38], in confirmation of an earlier claim [37]. We adopt this value along with the same helium abundance as in set A.

For the lithium abundance, we adopt the same value [45] as in Set B but increase the systematic error by 0.02 dex to allow for the uncertainty in the oscillator strengths of the lithium lines [51].

B. Qualitative Implications on N_ν and η

Different choices for the input data sets (A–D) lead to different implications for η and N_ν , that can be qualitatively understood through Figs. 1–4.

Figure 1 shows the BBN primordial abundances Y_i (solid lines) and their $\pm 2\sigma$ bands (dashed lines), as functions of $x \equiv \log(\eta/10^{-10})$, for $N_\nu = 2, 3$, and 4. The grey areas represent the $\pm 2\sigma$ bands allowed by the data set A (see Table I). There is global consistency between theory and data for $x \sim 0.2 - 0.4$ and $N_\nu = 3$, while for $N_\nu = 2$ ($N_\nu = 4$) the Y_2 data prefer values of x lower (higher) than the Y_4 data. Therefore, we expect that a global fit will favor values of (x, N_ν) close to $(0.3, 3)$.

Figure 2 is analogous, but for the data set B. In this case, there is still consistency between theory and data at $N_\nu = 3$, although for values of x higher than for the data set A. For $N_\nu = 2$ ($N_\nu = 4$) the combination of Y_2 and Y_7 data prefer values of x lower (higher) than Y_4 . The best fit is thus expected to be around $(x, N_\nu) \sim (0.7, 3)$.

Similarly, Figure 3 shows the abundances for the data set C. The situation is similar to data set B (Fig. 2), but one can envisage a best fit at a slightly lower value of x , due to the higher value of Y_2 , partly opposed by the increase in Y_7 .

Finally, Fig. 4 refers to the data set D. In this case, data and theory are not consistent for $N_\nu = 2$, since Y_2 and Y_4 pull x in different directions, and no “compromise” is possible since intermediate values of x are disfavored by Y_7 . However, for $N_\nu = 3$ there is relatively good agreement between data and theory at low x . Therefore, we expect a best fit around $(x, N_\nu) \sim (0.2, 3)$.

The qualitative indications discussed here are confirmed by a more accurate analysis, whose results are reported in the next section.

IV. DETERMINING N_ν

We now present the results of fits to the data sets A–D in the (x, N_ν) variables, using our method to estimate the correlated theoretical uncertainties, and adopting χ^2 statistics to include both theoretical and experimental errors. We have used the theoretical Y_i ’s obtained by the standard (updated) BBN evolution code [23], and checked that using the polynomial fits given in Sec. II B induce negligible changes which would not be noticeable on the plots.

In the analysis, we optionally take into account a further constraint on η (independent on N_ν) coming from a recent analysis of the Ly α -“forest” absorption lines in quasar spectra. The observed mean opacity of the lines requires some minimum amount of neutral hydrogen in the high redshift intergalactic medium, given a lower bound to the flux of ionizing radiation. Taking the latter from a conservative estimate of the integrated UV background due to quasars, Ref. [52] finds the constraint $\eta \geq 3.4 \times 10^{-10}$. This bound is not well-defined statistically but, for the sake of illustration, we have parametrized it through a penalty function quadratic in η :

$$\chi_{\text{Ly}\alpha}^2(\eta) = 2.7 \times \left(\frac{3.4 \times 10^{-10}}{\eta} \right)^2, \quad (10)$$

to be eventually added to the $\chi^2(\eta, N_\nu)$ derived from our fit to the elemental abundances. The above function excludes values of η smaller than 3.4×10^{-10} at 90% C.L. (for one degree of freedom, η).

Figure 5 shows the results of joints fits to $x = \log(\eta_{10})$ and N_ν using the abundances of data set A. The abundances Y_2 , Y_4 , and Y_7 are used separately (upper panels), in combinations of two (middle panels), and all together, without and with the Ly α -forest constraint on η (lower panels). In this way the relative weight of each piece of data in the global fit can be understood at glance. The three C.L. curves (solid, thick solid, and dashed) are defined by $\chi^2 - \chi_{\text{min}}^2 = 2.3, 6.2, \text{ and } 11.8$, respectively, corresponding to 68.3%, 95.4%, and 99.7% C.L. for two degrees of freedom (η and N_ν), i.e., to the probability intervals often designated as 1, 2, and 3 standard deviation limits. The χ^2 is minimized for each combination of Y_i , but the actual value of χ_{min}^2 (and the best-fit point) is shown only for the relevant global combination $Y_2 + Y_4 + Y_7(+\text{Ly}\alpha)$.

The results shown in Fig. 5 for the combinations Y_4+Y_7 and $Y_2+Y_4+Y_7$ are consistent with those obtained in ref. [29] by using the same input data but a completely different analysis

method (namely Monte Carlo simulation plus maximum likelihood). The consistency is reassuring and confirms the validity of our method. For this data set, the helium and deuterium abundances dominate the fit, as it can be seen by comparing the combinations $Y_2 + Y_4$ and $Y_2 + Y_4 + Y_7$. The preferred values of x are relatively low, and the preferred values of N_ν range between 2 and 4. Although the fit is excellent, the low value of x is in conflict with the Ly α -forest constraint on η , as indicated by the increase of χ_{\min}^2 from 0.02 to 8.89.

Figure 6 is analogous, but for the data set B which favors high values of x because of the ‘low’ deuterium abundance. The combination of $Y_2 + Y_7$ isolates, at high x , a narrow strip which depends mildly on N_ν . The inclusion of Y_4 selects the central part of such strip, corresponding to N_ν between 2 and 4. As in Fig. 5, the combination $Y_4 + Y_7$ does not appear to be very constraining. The overall fit to $Y_2 + Y_4 + Y_7$ is acceptable but not particularly good, mainly because Y_2 and Y_7 are only marginally compatible at high x . On the other hand, the $Y_2 + Y_4 + Y_7$ bounds are quite consistent with the Ly α -forest constraint.

In data set C, the deuterium abundance has increased further. Moreover the lithium abundance is no longer at the minimum of the theoretical curve as before, so strongly disfavors “intermediate” values of x . The overall effect, as shown in Figure 7, is that χ_{\min}^2 decreases a bit with respect to Set B, and the best fit value of x moves slightly lower. The allowed value of N_ν ranges between 2 and 4. Note that had we retained the same Y_7 as in Set B, then χ_{\min}^2 would have dropped to 0.91 (2.55) for the combination $Y_2 + Y_4 + Y_7$ (+ Ly α -forest constraint).

Finally, Fig. 8 refers to data set D which, like Data Set A, has the ‘high’ deuterium abundance but with larger uncertainties. So although a low value of x is still picked out, a high x region is still possible at the 2σ level (in the $Y_2 + Y_4 + Y_7$ panel) and is even favored when the Ly α -forest bound is included (although with an unacceptably high χ_{\min}^2). Note that had the lithium abundance been taken to be the same as in data set C (i.e. allowing for depletion), the χ_{\min}^2 would have been 0.07 (7.42) for the combination $Y_2 + Y_4 + Y_7$ (+ Ly α -forest constraint).

Of course one can also consider orthogonal combinations to those above, e.g. ‘high’ deuterium *and* ‘high’ helium, or ‘low’ deuterium *and* ‘low’ helium [30]. The latter combination implies $N_\nu \sim 2$, thus creating the so-called “crisis” for standard nucleosynthesis [18]. Conversely, the former combination suggests $N_\nu \sim 4$, which would also constitute evidence for new physics. Allowing for depletion of the primordial lithium abundance to its Pop II value, relaxes the upper bound on N_ν further, as noted earlier [24].

V. CONCLUSIONS

The results discussed above demonstrate that the present observational data on the primordial elemental abundances are not as yet sufficiently stable to derive firm bounds on η and N_ν . Different and arguably equally acceptable choices for the input data sets lead to very different predictions for η , and to relatively loose constraints on N_ν in the range 2 to 4 at the 95% C.L. Thus it may be premature to quote restrictive bounds based on some particular combination of the observations, until the discrepancies between different estimates are satisfactorily resolved. Our method of analysis provides the reader with an

easy-to-use technique [31] to recalculate the best-fit values as the observational situation evolves further.

However one might ask what would happen if these discrepancies remain? We have already noted the importance of an independent constraint on η (from the Ly α -forest) in discriminating between different options. However, given the many assumptions which go into the argument [52], this constraint is rather uncertain at present. Fortunately it should be possible in the near future to independently determine η to within $\sim 5\%$ through measurements of the angular anisotropy of the cosmic microwave background (CMB) on small angular scales [53], in particular with data from the all-sky surveyors MAP and PLANCK [54]. Such observations will also provide a precision measure of the relativistic particle content of the primordial plasma. Hopefully the primordial abundance of ${}^4\text{He}$ would have stabilized by then, thus providing, in conjunction with the above measurements, a reliable probe of a wide variety of new physics which can affect nucleosynthesis.

ACKNOWLEDGMENTS

We thank G. Fiorentini for useful discussions and for earlier collaboration on the subject of this paper.

REFERENCES

- [1] For a recent review, see J. Conrad, hep-ex/9811009, plenary talk at the Intern. Conf. on High Energy Physics, Vancouver (1998).
- [2] C. Caso *et al.* (Particle Data Group), Eur. J. Phys. C **3**, 1 (1998).
- [3] F. Hoyle and R.J. Tayler, Nature **203**, 1108 (1964); P.J.E. Peebles, Phys. Rev. Lett. **16**, 411 (1966); V.F. Shvartsman, Pis'ma Zh. Eksp. Teor. Fiz. **9**, 315 (1969) [JETP Lett. **9**, 184 (1969)].
- [4] G. Steigman, D.N. Schramm, and J. Gunn, Phys. Lett. **66B**, 202 (1977); G. Steigman, K.A. Olive, and D.N. Schramm, Phys. Rev. Lett. **43**, 239 (1979).
- [5] K.A. Olive, D.N. Schramm, and G. Steigman, Nucl. Phys. B **180**, 497 (1981).
- [6] K. Enqvist, K. Kainulainen and M. Thomson, Nucl. Phys. B **373**, 498 (1992).
- [7] D.P. Kirilova and M.V. Chizhov, Nucl. Phys. B **534**, 447 (1998); R. Foot and R.R. Volkas, Phys. Rev. D **55**, 5147 (1997).
- [8] A.D. Dolgov, S.H. Hansen, S. Pastor, and D.V. Semikoz, hep-ph/9809598; S. Hannestad, Phys. Rev. D **57**, 2213 (1998); M. Kawasaki, K. Kohri and K. Sato, Phys. Lett. B **430**, 132 (1998).
- [9] A.D. Dolgov, S. Pastor, J.C. Romão, and J.W.F. Valle, Nucl. Phys. B **496**, 24 (1997).
- [10] R. Lopez and M.S. Turner, astro-ph/9807279, to appear in Phys. Rev. D.
- [11] B.E.J. Pagel, E.A. Simonson, R.J. Terlevich, and M.G. Edmunds, Mon. Not. R. Astr. Soc. **255**, 325 (1992); K.A. Olive and G. Steigman, Astrophys. J. Suppl. **97**, 49 (1995).
- [12] Y.I. Izotov, T.X. Thuan, and V. A. Lipovetsky, Astrophys. J. **435**, 647 (1994), Astrophys. J. Suppl. **108**, 1 (1997).
- [13] R. Epstein, J. Lattimer, and D.N. Schramm, Nature **263**, 198 (1976).
- [14] A. Songaila, L.L. Cowie, C.J. Hogan and M. Rugers, Nature **368**, 599 (1994); R.F. Carswell, M. Rauch, R.J. Weymann, A.J. Cooke, and J.K. Webb, Mon. Not. R. Astr. Soc. **268**, L1 (1994); M. Rugers and C.J. Hogan, Astrophys. J. Lett. **459**, L1 (1996), Astron. J. **111**, 2135 (1996).
- [15] D. Tytler, X-M. Fan, and S. Burles, Nature **381**, 207 (1996); S. Burles and D. Tytler, Astron. J. **114**, 1330 (1997).
- [16] S. Sarkar, Rep. Prog. Phys. **59**, 1493 (1996).
- [17] J. Yang, M.S. Turner, G. Steigman, D.N. Schramm, and K.A. Olive, Astrophys. J. **281**, 493 (1984); G. Steigman, K.A. Olive, D.N. Schramm, and M.S. Turner, Phys. Lett. B **176**, 33 (1986); K.A. Olive, D.N. Schramm, G. Steigman, and T.P. Walker, Phys. Lett. B **236**, 454 (1990); T.P. Walker, G. Steigman, D.N. Schramm, K.A. Olive, and H.-S. Kang, Astrophys. J. **376**, 51 (1991).
- [18] N. Hata, R.J. Scherrer, G. Steigman, D. Thomas, T.P. Walker, S. Bludman and P. Langacker, Phys. Rev. Lett. **75**, 3977 (1995).
- [19] J. Ellis, K. Enqvist, D.V. Nanopoulos, and S. Sarkar, Phys. Lett. B **167**, 457 (1986).
- [20] P.J. Kernan and L.M. Krauss, Phys. Rev. Lett. **72**, 3309 (1994); L.M. Krauss and P.J. Kernan, Astrophys. J. Lett. **432**, L79 (1994), Phys. Lett. B **347**, 347 (1995).
- [21] L.M. Krauss and P. Romanelli, Astrophys. J. **358**, 47 (1990);
- [22] M.S. Smith, L.H. Kawano, and R. A. Malaney, Astrophys. J. Suppl. **85**, 219 (1993).
- [23] R.V. Wagoner, Astrophys. J. **179**, 343 (1973); L. Kawano, Report No. Fermilab-Pub-88/34-A, 1988 (unpublished), Report No. Fermilab-Pub-92/04-A, 1992 (unpublished).
- [24] P.J. Kernan and S. Sarkar, Phys. Rev. D **54**, R3681 (1996).

- [25] C.J. Copi, D.N. Schramm, and M.S. Turner, Phys. Rev. D**55**, 3389 (1997).
- [26] B.D. Fields and K.A. Olive, Phys. Lett. B **368**, 103 (1996); B.D. Fields, K. Kainulainen, K.A. Olive, and D. Thomas, New Astron. **1**, 77 (1996).
- [27] N. Hata, G. Steigman, S. Bludman, and P. Langacker, Phys. Rev. D**55**, 540 (1997).
- [28] G. Fiorentini, E. Lisi, S. Sarkar, and F.L. Villante, Phys. Rev. D**58**, 063506 (1998).
- [29] K.A. Olive and D. Thomas, Astropart. Phys. **7** (1997) 27.
- [30] E. Holtman, M. Kawasaki, K. Kohri, and T. Moroi, hep-ph/9805405.
- [31] See: <http://www-thphys.physics.ox.ac.uk/users/SubirSarkar/bbn.html>
- [32] R. Esmailzadeh, G.D. Starkman, and S. Dimopoulos, Astrophys. J. **378**, 504 (1991).
- [33] J.A. Bernstein, L.S. Brown, and G. Feinberg, Rev. Mod. Phys. **61**, 25 (1989).
- [34] B.E.J. Pagel, *Nucleosynthesis and the Chemical Evolution of Galaxies* (Cambridge University Press, Cambridge, 1997).
- [35] C. Hogan, Sp. Sci. Rev. **84**, 127 (1998).
- [36] P. Molaro, in *From Quantum Fluctuations to Cosmological Structures*, edited by D. Valls-Gabaud *et al.*, ASP Conf. Ser. **126**, 103 (1997).
- [37] J.K. Webb, R.F. Carswell, K.M. Lanzetta, R. Ferlet, M. Lemoine, and A. Vidal-Madjar, Nature **388**, 250 (1997).
- [38] D. Tytler, S. Burles, L. Lu, X-M. Fan, A. Wolfe and B.D. Savage, astro-ph/9810217, to appear in Astron. J.
- [39] S. Burles and D. Tytler, Astrophys. J. **499**, 699 (1998).
- [40] S. Burles and D. Tytler, Astrophys. J. **507**, 732 (1998); Sp. Sci. Rev. **84**, 65 (1998).
- [41] K.A. Olive, G. Steigman, and E.D. Skillman, Astrophys. J. **483**, 788 (1997).
- [42] Y.I. Izotov and T.X. Thuan, Astrophys. J. **497**, 227 (1998); **500**, 188 (1998).
- [43] S.G. Ryan, T.C. Beers, C.P. Deliyannis, and J. Thorburn, Astrophys. J. **458**, 543 (1996).
- [44] P. Molaro, F. Primas, and P. Bonifacio, Astron. Astrophys. **295**, L47 (1995).
- [45] P. Bonifacio and P. Molaro, Mon. Not. Roy. Astron. Soc. **285**, 847 (1997).
- [46] M.H. Pinsonneault, C.P. Deliyannis, and P. Demarque, Astrophys. J. Suppl. **78**, 179 (1992).
- [47] S. Vauclair and C. Charbonnel, Astron. Astrophys. **295**, 715 (1995); astro-ph/9802315, to appear in Astrophys. J.
- [48] P. Bonifacio and P. Molaro, Astrophys. J. Lett. **500**, L175 (1998).
- [49] S.A. Levshakov, W.H. Kegel, and F. Takahara, Astrophys. J. **499**, L1 (1998); Astron. and Astrophys. **336**, L29 (1998); S.A. Levshakov, D. Tytler, and S. Burles, astro-ph/9812114.
- [50] M.H. Pinsonneault, T.P. Walker, G. Steigman, and V.K. Narayanan, astro-ph/9803073.
- [51] P. Molaro, private communication.
- [52] D.H. Weinberg, J. Miralda-Escudé, L. Hernquist, and N. Katz, Astrophys. J. **490**, 564 (1997).
- [53] For a review, see, D.N. Spergel, Proc. Nobel Symp.: *Particle Physics and the Universe*, Enkoping, Sweden, August 20-25, 1998, to be published in Phys. Scripta.
- [54] MAP: <http://map.gsfc.nasa.gov/>;
PLANCK: <http://astro.estec.esa.nl/SA-general/Projects/Planck/>

TABLES

TABLE I. Experimental data sets considered in this paper for the elemental abundances Y_i .

	A	B	C	D
$Y_2 \times 10^5$	19 ± 4	3.4 ± 0.3	4.35 ± 0.43	33 ± 12
Y_4	0.234 ± 0.0054	0.245 ± 0.004	0.245 ± 0.004	0.234 ± 0.0054
$Y_7 \times 10^{10}$	1.6 ± 0.36	1.73 ± 0.21	3.9 ± 0.85	1.73 ± 0.29

FIGURES

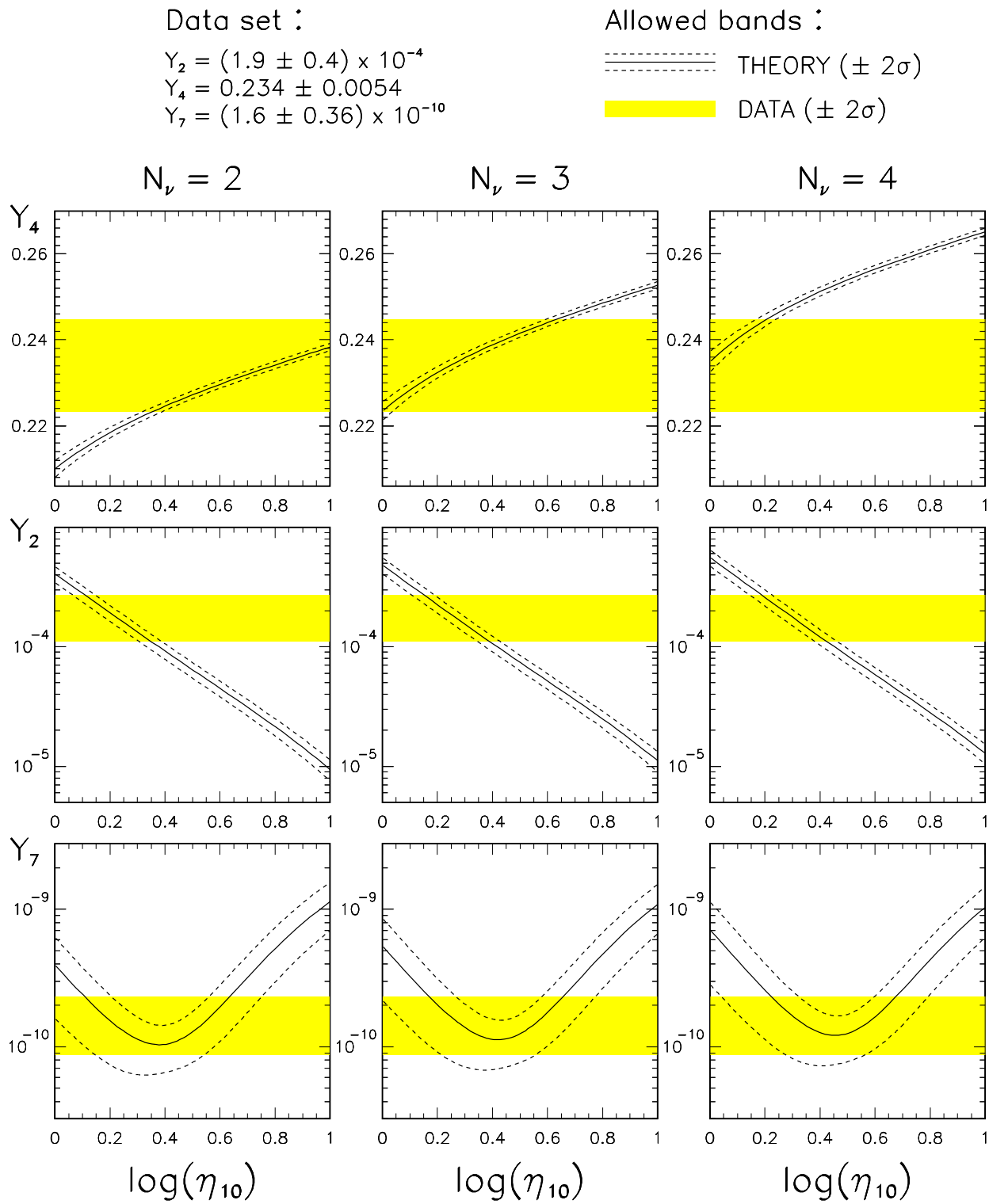


FIG. 1. Primordial abundances Y_4 (${}^4\text{He}$ mass fraction) Y_2 (D/H) and Y_7 (${}^7\text{Li}$ /H), for $N_\nu = 2, 3,$ and 4 . Solid and dashed curves represent the theoretical central values and the $\pm 2\sigma$ bands, respectively. The grey areas represent the $\pm 2\sigma$ experimental bands for the data set A in Table I.

Data set :

$$Y_2 = (3.4 \pm 0.3) \times 10^{-5}$$

$$Y_4 = 0.245 \pm 0.004$$

$$Y_7 = (1.73 \pm 0.21) \times 10^{-10}$$

Allowed bands :

----- THEORY ($\pm 2\sigma$)

DATA ($\pm 2\sigma$)

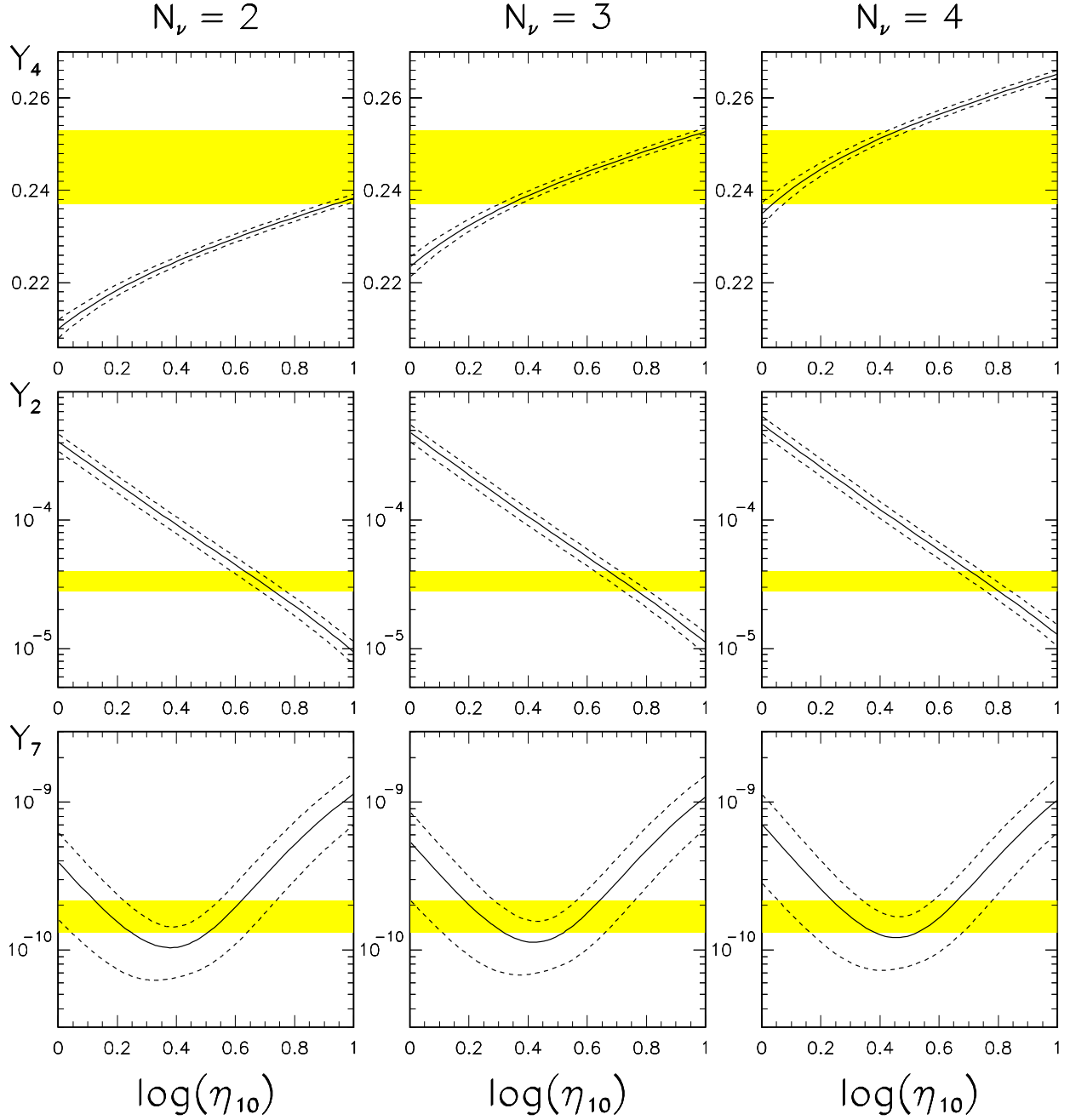


FIG. 2. As in Fig. 1, but for the data set B.

Data set :

$$Y_2 = (4.35 \pm 0.43) \times 10^{-5}$$

$$Y_4 = 0.245 \pm 0.004$$

$$Y_7 = (3.9 \pm 0.85) \times 10^{-10}$$

Allowed bands :

----- THEORY ($\pm 2\sigma$)

DATA ($\pm 2\sigma$)

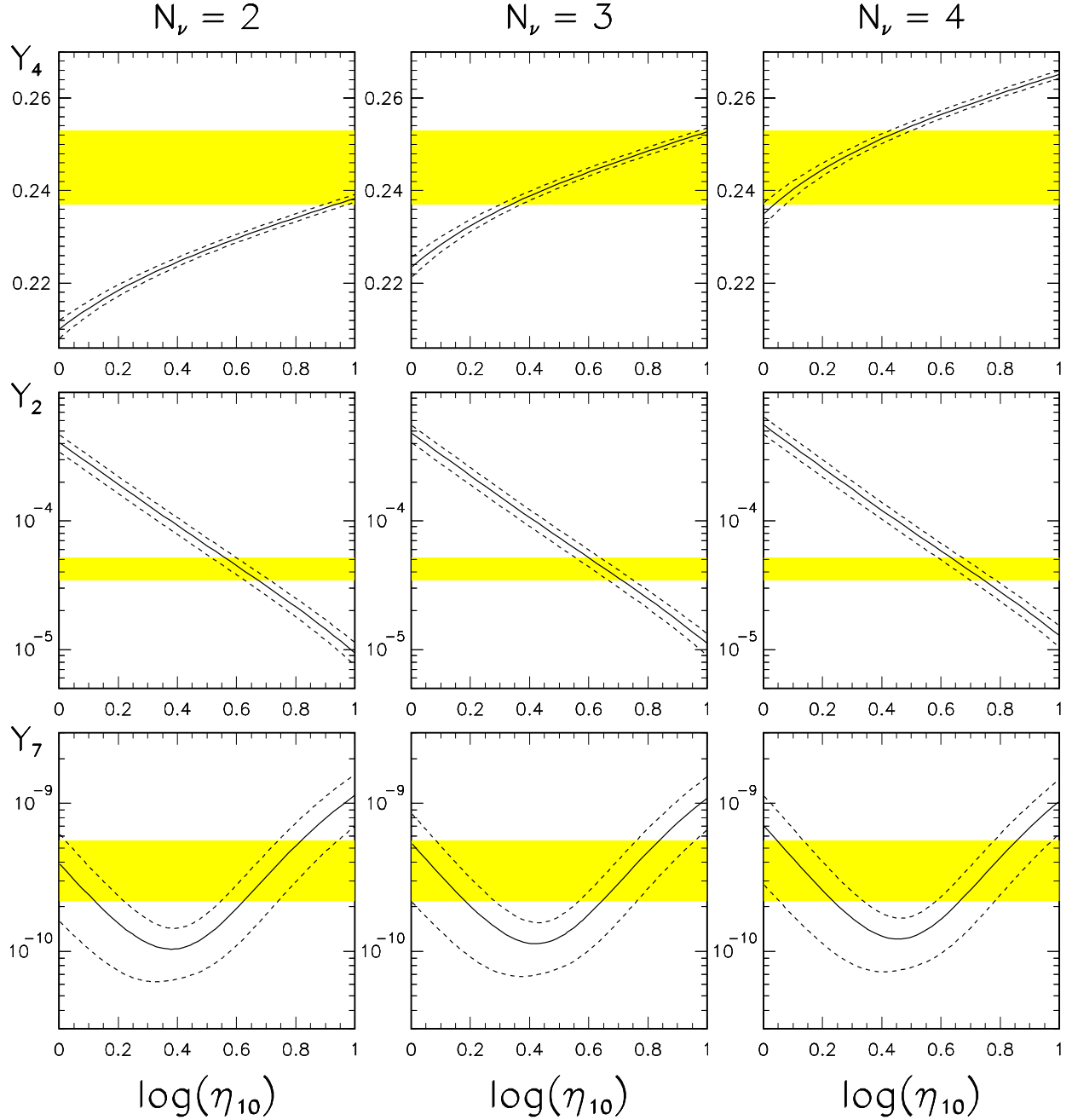


FIG. 3. As in Fig. 1, but for the data set C.

Data set :

$$Y_2 = (3.3 \pm 1.2) \times 10^{-4}$$

$$Y_4 = 0.234 \pm 0.0054$$

$$Y_7 = (1.73 \pm 0.29) \times 10^{-10}$$

Allowed bands :

----- THEORY ($\pm 2\sigma$)

DATA ($\pm 2\sigma$)

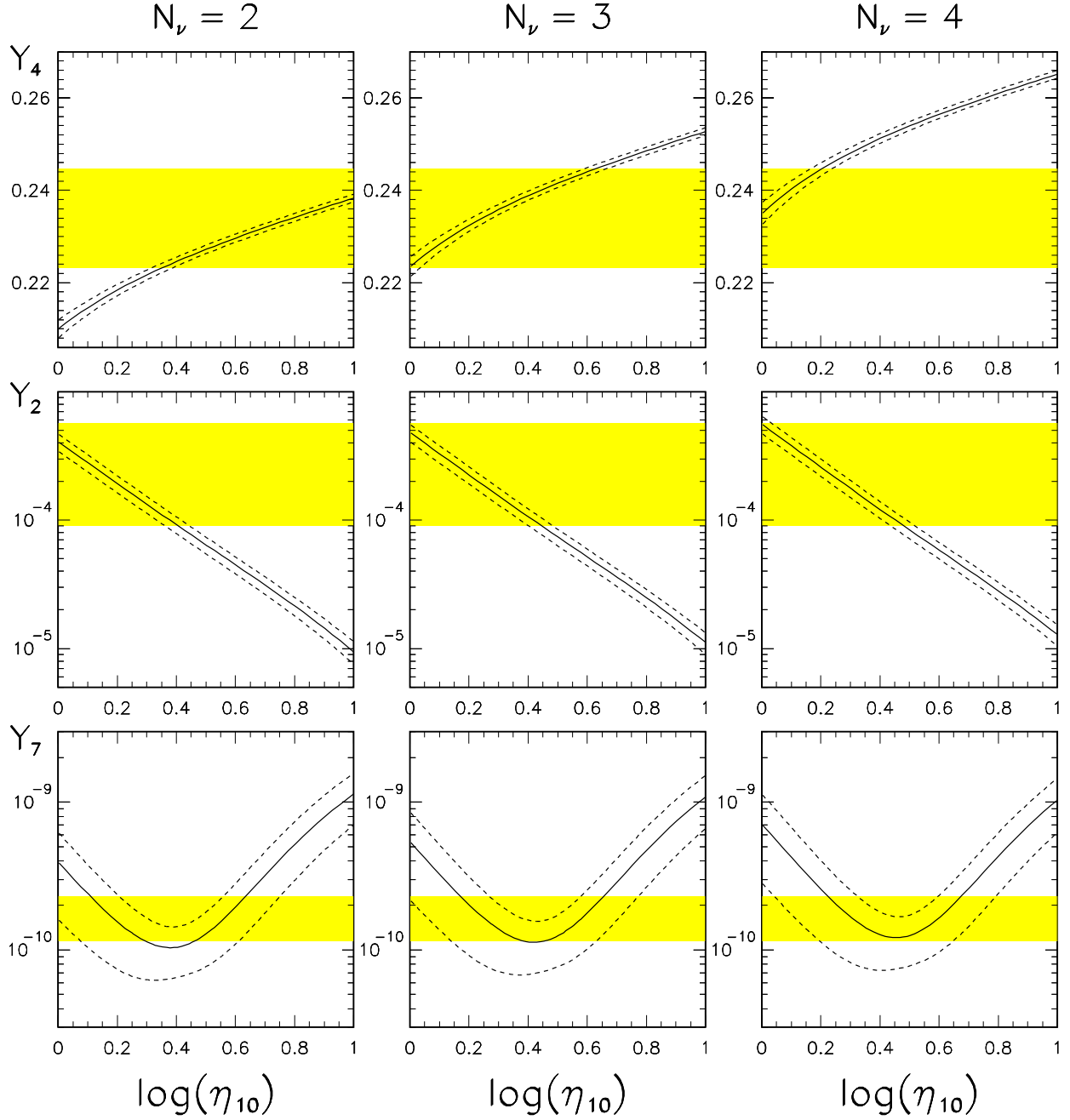


FIG. 4. As in Fig. 1, but for the data set D.

Data set :

$$Y_2 = (1.9 \pm 0.4) \times 10^{-4}$$

$$Y_4 = 0.234 \pm 0.0054$$

$$Y_7 = (1.6 \pm 0.36) \times 10^{-10}$$

Allowed regions :

———— 68.3% C.L.
 ———— 95.4% C.L.
 ······ 99.7% C.L.

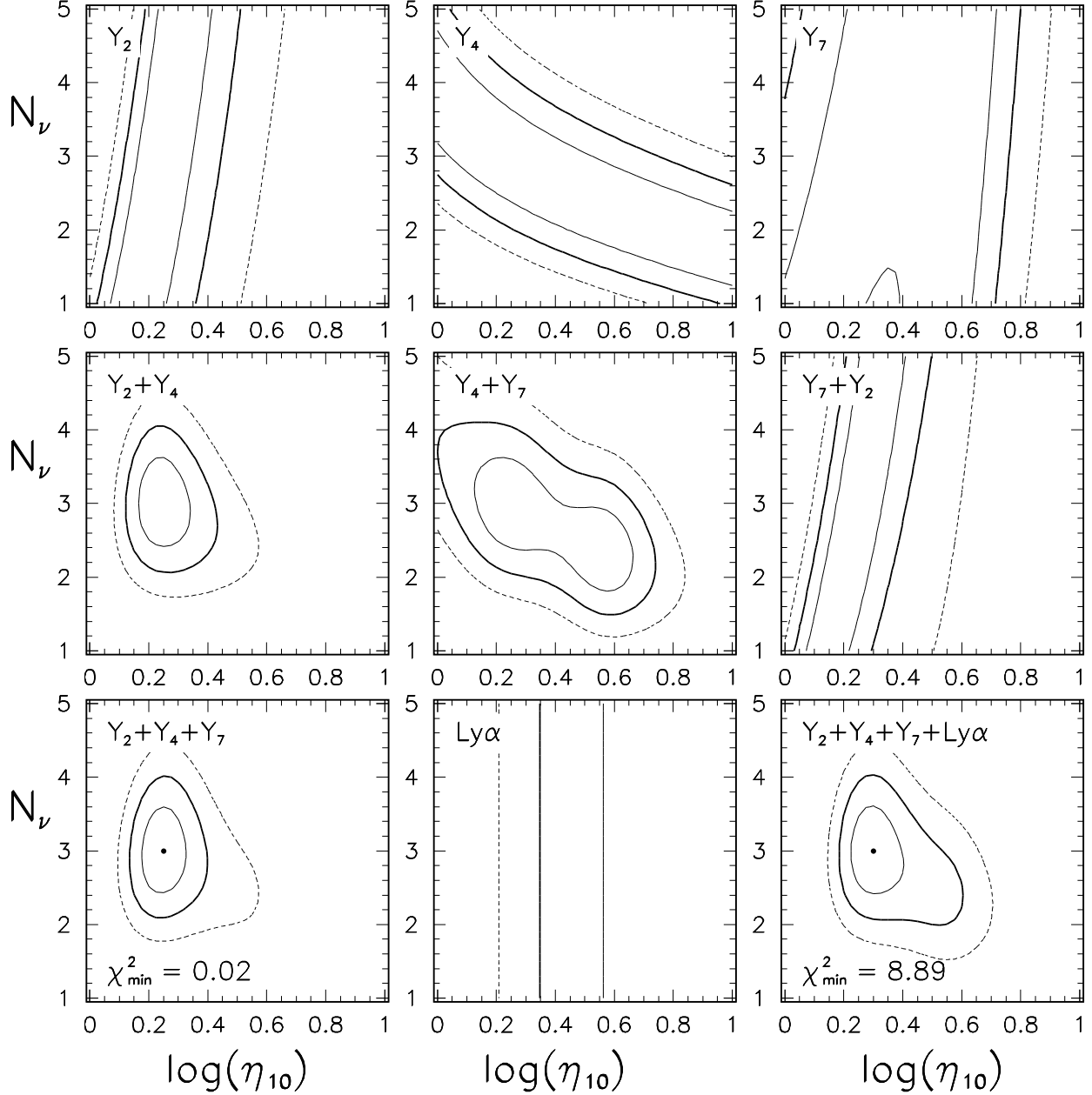


FIG. 5. Joint fits to $x = \log(\eta_{10})$ and N_ν using the abundances of data set A. The abundances Y_2 , Y_4 , and Y_7 are used separately (upper panels), in combinations of two (middle panels), and all together, without and with the $\text{Ly}\alpha$ -forest constraint on η (lower panels).

Data set :

$$Y_2 = (3.4 \pm 0.3) \times 10^{-5}$$

$$Y_4 = 0.245 \pm 0.004$$

$$Y_7 = (1.73 \pm 0.21) \times 10^{-10}$$

Allowed regions :

———— 68.3% C.L.
 ———— 95.4% C.L.
 ······ 99.7% C.L.

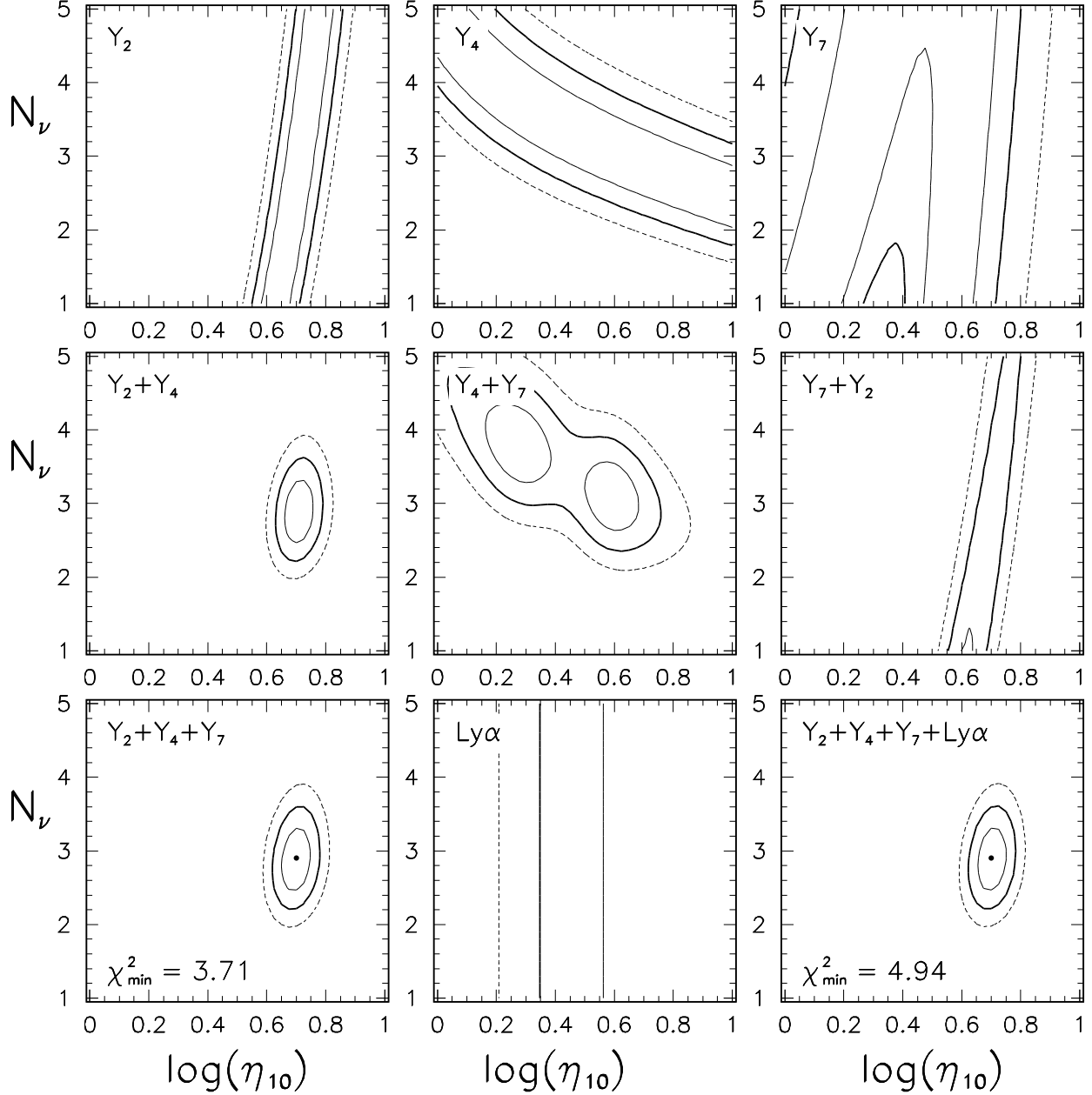


FIG. 6. As in Fig. 5, but for the data set B.

Data set :

$$Y_2 = (4.35 \pm 0.43) \times 10^{-5}$$

$$Y_4 = 0.245 \pm 0.004$$

$$Y_7 = (3.90 \pm 0.85) \times 10^{-10}$$

Allowed regions :

————— 68.3% C.L.
 ————— 95.4% C.L.
 - - - - - 99.7% C.L.

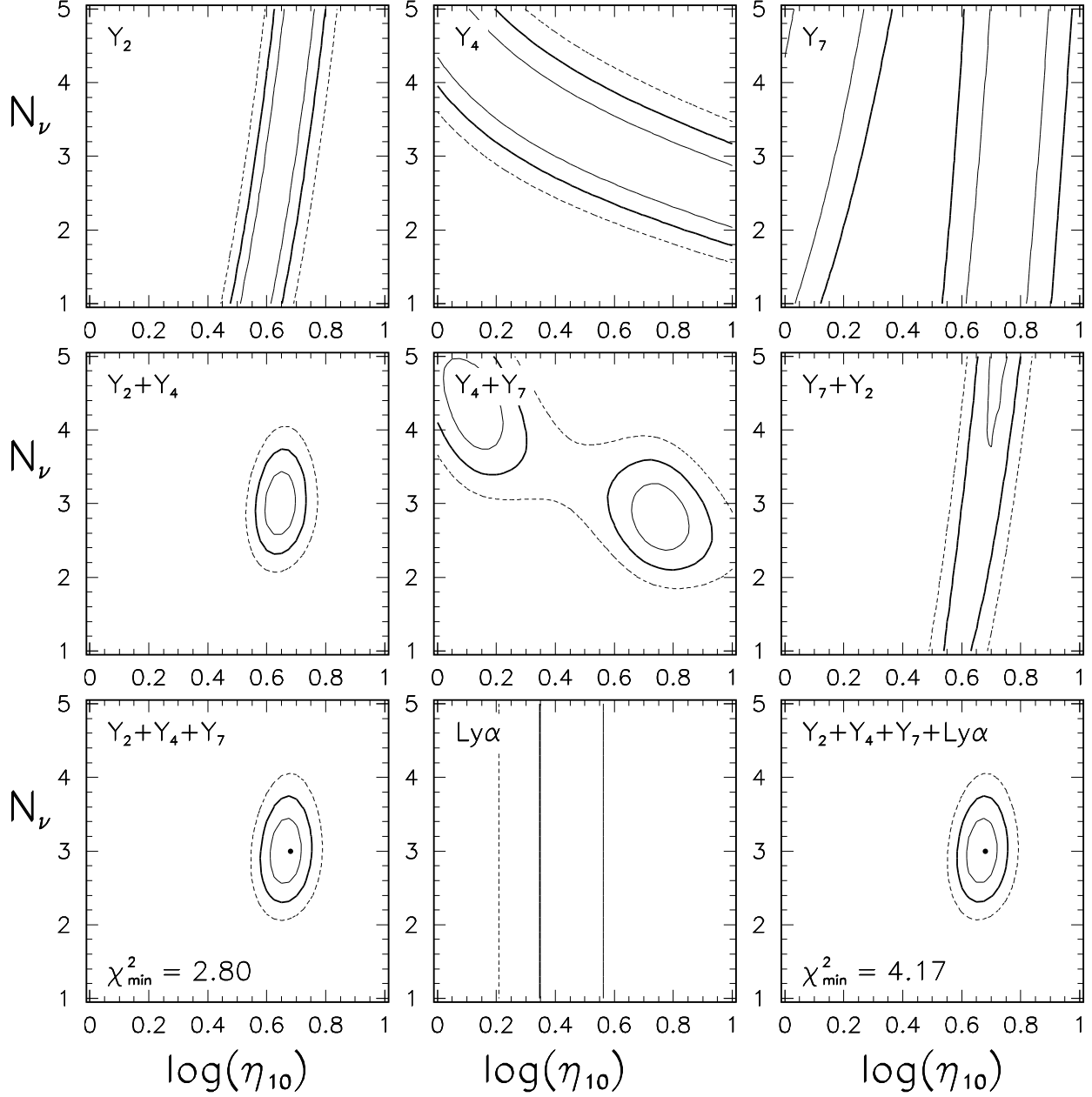


FIG. 7. As in Fig. 5, but for the data set C.

Data set :

$$Y_2 = (3.3 \pm 1.2) \times 10^{-4}$$

$$Y_4 = 0.234 \pm 0.0054$$

$$Y_7 = (1.73 \pm 0.29) \times 10^{-10}$$

Allowed regions :

— 68.3% C.L.
 — 95.4% C.L.
 - - - 99.7% C.L.

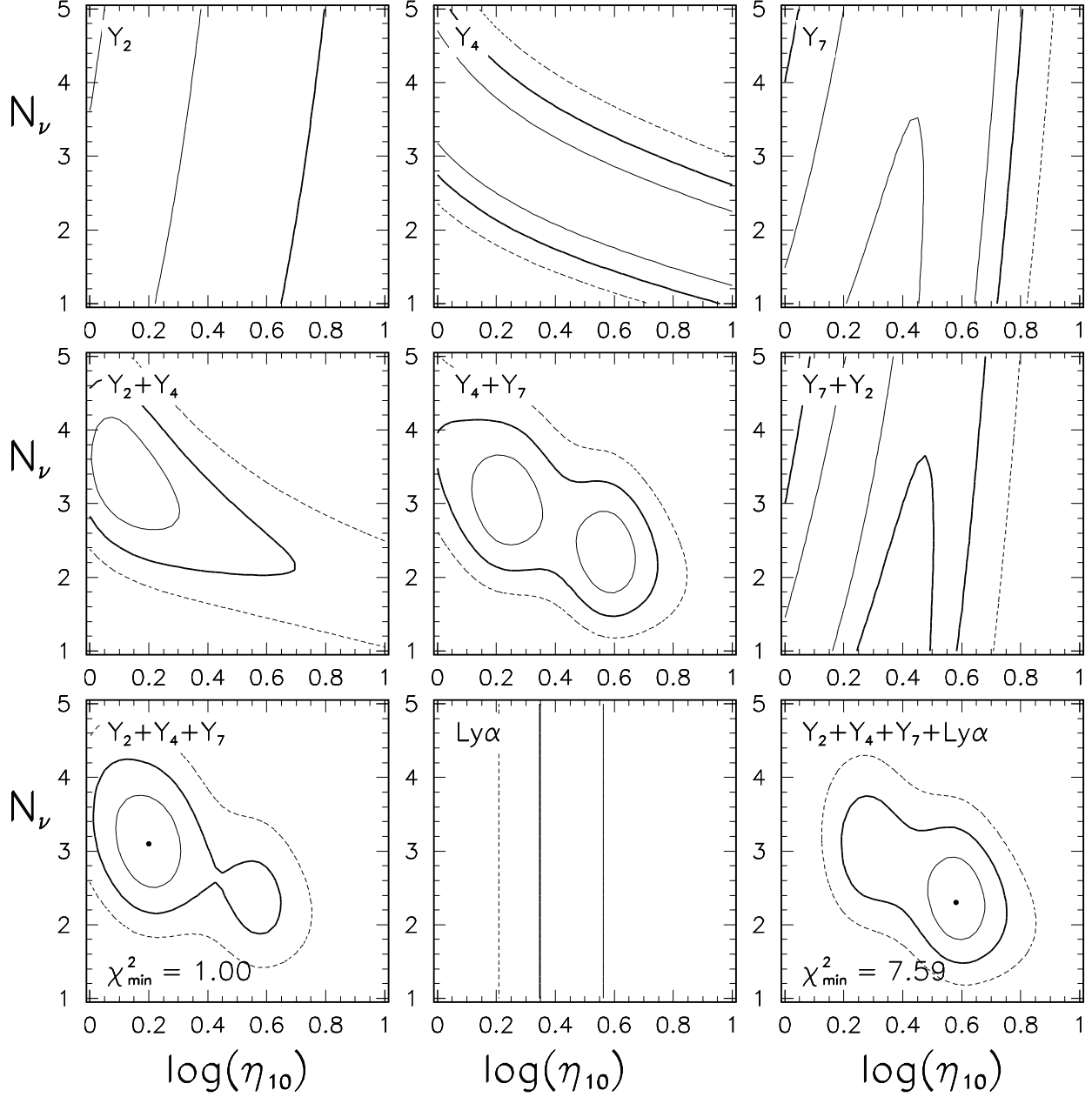


FIG. 8. As in Fig. 5, but for the data set D.